Crack initiation in PMMA plates with circular holes considering kinetic energy and nonlinear elastic material behaviour

Xi Chen, Aurélien Doitrand, Nathalie Godin, Claudio Fusco

▶ **To cite this version:**

Xi Chen, Aurélien Doitrand, Nathalie Godin, Claudio Fusco. Crack initiation in PMMA plates with circular holes considering kinetic energy and nonlinear elastic material behaviour. Theoretical and Applied Fracture Mechanics, 2023, pp.103783. 10.1016/j.tafmec.2023.103783 . hal-03955880

HAL Id: hal-03955880
https://hal.science/hal-03955880

Submitted on 25 Jan 2023

HAL is a multi-disciplinary open access archive for the deposit and dissemination of scientific research documents, whether they are published or not. The documents may come from teaching and research institutions in France or abroad, or from public or private research centers.

L'archive ouverte pluridisciplinaire **HAL**, est destinée au dépôt et à la diffusion de documents scientifiques de niveau recherche, publiés ou non, émanant des établissements d'enseignement et de recherche français ou étrangers, des laboratoires publics ou privés.

Crack initiation in PMMA plates with circular holes considering kinetic energy and nonlinear elastic material behaviour

Xi Chen[a,*], Aurélien Doitrand[a], Nathalie Godin[a], Claudio Fusco[a]

[a] *Univ Lyon, INSA Lyon, UCBL, CNRS, MATEIS, UMR5510, 69621, Villeurbanne, France*

Abstract

The coupled criterion (CC) of finite fracture mechanics (FFM) is extended to assess crack initiation in PMMA specimens with holes under quasi-static loading considering nonlinear elastic (NLE) material model and considering the kinetic energy variation in the energy balance. If dynamic aspects are disregarded, the failure stress predicted using the CC for either linear elastic (LE) material model or NLE material model is underestimated compared to the one measured experimentally. A better representation of the failure stress variation as a function of the hole size is obtained considering constant crack velocity profiles and velocities in the range [550-900] m/s (LE material model) or [400-600] m/s (NLE material model). The predicted failure stresses also depend on the crack velocity profile.

Keywords: Coupled Criterion, Nonlinearity, Dynamic approach, Crack initiation

1. Introduction

Crack nucleation in brittle or quasi-brittle materials can be investigated within the framework of finite fracture mechanics (FFM) [1, 2], which consists of considering finite rather than infinitesimal crack increments as in linear elastic fracture mechanics (LEFM) approach [3]. FFM overcomes a main LEFM limitation concerning crack initiation study [1, 2]. To achieve a prediction of crack initiation, Leguillon [4] proposed the coupled criterion (CC), which is based on the simultaneous fulfillment of two separate conditions: on the one hand, the stress must be larger than the material tensile strength over a finite length; on the other hand, the incremental energy release rate (IERR) must be larger than the crack surface creation energy. The stress field and IERR can be obtained either from analytical functions [5], based on matched asymptotic expansions [4] or by means of finite element (FE) simulations [6].

The CC can be applied to crack initiation prediction in various configurations, such as, at V-notches [7, 8] or interfaces [9, 10]. Crack initiation at a circular hole was studied using the CC by analytical approach or semi-analytical approach [11–15]. Weiβgraeber et al. [11] set up a closed-form analytical CC formulation to solve the crack initiation problem of plates containing ellipse holes. They showed that the failure load and the asymmetric crack pattern exhibited a dependence on the hole size and elliptical aspect ratio. Sapora and Cornetti [12] investigated crack initiation from a circular hole in an infinite plate under biaxial loading

*Fully documented templates are available in the elsarticle package on CTAN.

*Corresponding author
Email address: xi.chen@insa-lyon.fr (Xi Chen)

and the stability of crack propagation depending on the loading biaxiality and crack advance to hole radius ratio. Rosendahl et al. [13] studied the crack initiation symmetry or asymmetry at a centered hole in a plate under combined tension and bending loading. They revealed that crack initiation at the hole edge or at the specimen free edge depended on the hole size and bending to tensile stress ratio. Doitrand et al. [16] studied the asymmetric crack initiation at a cylindrical hole located near a free edge. They highlighted that either simultaneous or unilateral crack initiation occurred depending on the ligament size compared to the material characteristic length. The CC was also used to assess crack initiation in PMMA specimens containing a circular hole under tensile loading, which enabled to estimate the failure stress variation as a function of the hole size [17–19]. The critical failure load varied between the material tensile strength for small hole to one third of it when then hole size was large enough [17, 18]. This variation was however not obtained for materials exhibiting sufficiently marked nonlinearities [19].

The CC was also applied to predict crack initiation considering geometrical or material nonlinearities, for instance under moderate or large scale yielding regimes [20]. Talmon et al. [21] studied the IERR of composite single-lap joints using a nonlinear crack opening integral and quantified the difference on the incremental and differential energy release rate compared to the linear case. The influence of the geometrical nonlinearity on the fracture stress in the same configuration was studied by Wei et al. [22]. They highlighted that the consideration of the nonlinearity improved the fracture stress prediction and the IERR in the nonlinear analysis decreased significantly, compared to an overestimated IERR in the linear analysis. Leguillon et al. [23] extended the CC to consider a small plastic or damaged zone ahead of a V-notch in quasi-brittle materials. A damage model was used to represent the Young's modulus decrease in the damage zone. Varying tensile strength and fracture toughness were also considered. Yosibash et al. [24] highlighted that the classical approach of the CC underestimated the failure force of quasi-brittle steel alloys because of the plastic zone ahead of the V-notch tip. Rosendahl et al. [25] coupled equivalent average strain and energy criteria to study crack initiation of a structural silicone adhesive, using the hyperelastic Marlow-type material model. The nonlinear FFM implementation allowed an improvement of the predicted failure stress of Brazilian disk specimen with a hole compared to measured one, especially for small holes [6]. The Ramberg-Osgood (RO) model was also used to describe the nonlinear constitutive behavior [6, 19].

Leite et al. [19] considered the nonlinearity of PMMA to study crack initiation at a circular hole, by experiments and using FFM. PMMA elastic and fracture properties were determined by carrying out tensile tests on plain specimens as well as single edge notch bending. Then, tensile tests were carried out on plates with a circular hole to study crack initiation at the hole. The fracture stress for different hole diameters (from 0.5 mm to 10 mm) and the average crack velocities for the left and right cracks were measured. It was shown that the fracture stresses decreased with increasing hole diameters. The CC for linear elastic (LE) and non-linear elastic (NLE) material model were used to predict the crack onset of two symmetric cracks at a circular hole of a stretched PMMA plate, resulting in predicted failure stresses smaller than those measured experimentally. Actually, minor differences were obtained using NLE material behavior compared to the failure stress variation obtained using CC approach for LE case. Therefore, no significant improvement of the agreement between the predictions and the experimental results was obtained considering nonlinearities.

This underestimate may be explained by the use of a quasi-static CC approach, which predicts that crack nucleation occurs instantaneously over a given length at a given loading level, disregarding the dynamic formation of the newly created crack. Noteworthy, Laschuetza and Seelig [15] highlighted the fact that the quasi-static CC approach predicted excess of energy release rate to critical energy release rate ratio at crack initiation, which may possibly lead to underestimating the failure load. Extending the CC to dynamic crack nucleation was pointed out as a challenge in the paper review by Weiβgraeber et al. [11]. Since then, few papers addressed dynamic aspects of crack initiation [15, 26, 27]. An extension of the CC considering dynamic crack nucleation was recently addressed [28]. Compared with the classical quasi-static approach, the crack velocity profile was considered instead of an instantaneous crack initiation as well as the kinetic energy creation due to crack nucleation. The value of IERR using CC dynamic approach decreased compared to the value obtained using quasi-static approach when the crack velocity increased [28], which may thus lead to an increase in the predicted fracture stress provided the actual crack velocity is large enough.

The objective of this work is to consider both nonlinearities and CC dynamic approach to study crack initiation at a circular hole in PMMA specimens. The CC quasi-static approach for LE and NLE material models as well as the CC dynamic approach for LE material model are recalled and the CC dynamic approach is extended for NLE case in Section 2. The computational set-up of CC is presented in Section 3. Then, the CC dynamic approach for LE case and NLE case are both applied to assess crack initiation under quasi-static loading in a infinite plate with a circular hole and the results are compared to the experimental results of Leite et al. [19] in Section 4.

2. The coupled criterion

A schematic representation of the geometry and loading under investigation in uncracked and cracked specimens is shown in Fig. 1. The length L and the width W of the holed plate are 300 mm and 40 mm respectively. The hole diameters are ϕ = 2 R = 0.5, 1.0, 2.0, 3.0, 4.25 and 10 mm. The material employed is an amorphous thermoplastic polymer, Polymethyl Metacrylate (PMMA). The material properties determined in [19] are given in Table 1.

E	ν	ρ	σ_c	$\mathcal{G}_c$
3000 MPa	0.34	1100 kg/m^3	63.4 MPa	496 J/m^2

Table 1: Material properties of PMMA [19]

In this section, we start from the general concept of the CC. Then, we extend it considering both nonlinearities and dynamic aspects. The CC is based on the simultaneous fulfillment of stress and energy requirements. The first requirement of the CC states that the stress is larger than the tensile strength σ_c all along the crack path before crack initiation, which is written as:

$$\sigma(\ell, U) \geqslant \sigma_c \quad \forall\, 0 \leqslant \ell \leqslant \ell_c, \tag{1}$$

where ℓ is the crack length. U, the imposed loading or displacement and ℓ_c, the initiation crack length, are the two problem unknowns. The second requirement is based on the principle of energy conservation between

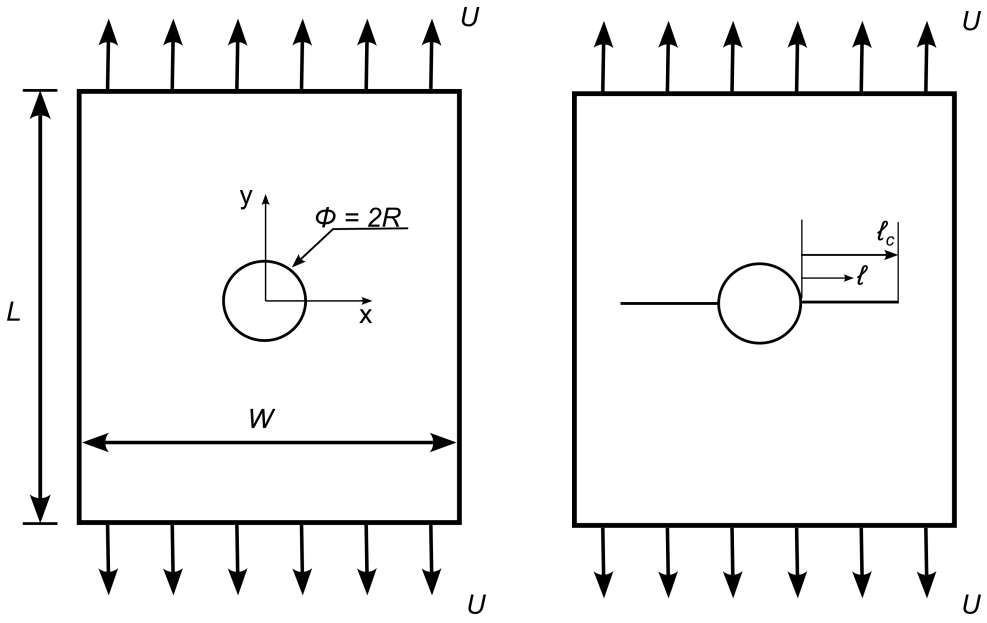

Figure 1: Geometry and loading of the plate (a) before crack initiation, (b) after symmetrical crack initiation.

the states prior to and after crack initiation. It is obtained by a balance of the variation in the external force work (W_{ext}), elastic strain energy (W_p), kinetic energy (W_k), and crack surface creation energy ($\mathcal{G}_c\ell$, where $\mathcal{G}_c$ is the material fracture toughness and ℓ is the crack length):

$$\Delta W_{ext}(\ell, U) - \Delta W_p(\ell, U) - \Delta W_k(\ell, U) = \mathcal{G}_c\ell \tag{2}$$

According to the CC, crack initiation can only occur provided the two requirements given in Eqs. (1) and (2) as two functions of ℓ and U are simultaneously fulfilled. Solving the CC thus reverts to determining the minimum imposed displacement and crack length satisfying both Eqs. (1) and (2).

2.1. Quasi-static approach for Linear Elastic material model

Based on the quasi-static approach, cracks are assumed to initiate instantaneously. Under quasi-static loading, the kinetic energy is null prior to crack initiation, which results in an increase in kinetic energy $\Delta W_k \geqslant 0$. Therefore, the energy balance in Eq. (2) turns into the following inequality:

$$\mathcal{G}_{inc}(\ell, U) = \frac{\Delta W_{ext}(\ell, U) - \Delta W_p(\ell, U)}{\ell} \geqslant \mathcal{G}_c, \tag{3}$$

where $\mathcal{G}_{inc}$ is the incremental energy release rate (IERR). Note that, for the case of prescribed displacements, $\Delta W_{ext} = 0$ and thus, $\mathcal{G}_{inc} = -\Delta W_p/\ell$. Using a LE material model and small deformation assumption, the stress is proportional to the prescribed displacement and the IERR is proportional to the square of prescribed displacement [28]:

$$\begin{cases} G_{inc}(\ell, U) = A(\ell)U^2 \geqslant \mathcal{G}_c, \\ \sigma(\ell, U) = k(\ell)U \geqslant \sigma_c, \end{cases} \tag{4}$$

where $A(\ell)$ and $k(\ell)$ are functions depending on the problem geometry.

Based on Eq. (4), the minimum loading level at crack initiation U_c and the initiation crack length ℓ_c can be determined as:

$$\begin{cases} U_c = \min\limits_{\ell} \left\{ \max \left(\sqrt{\frac{\mathcal{G}_c}{A(\ell)}}, \frac{\sigma_c}{k(\ell)} \right) \right\} \\ \ell_c = \operatorname*{argmin}\limits_{\ell} \left\{ \max \left(\sqrt{\frac{\mathcal{G}_c}{A(\ell)}}, \frac{\sigma_c}{k(\ell)} \right) \right\} \end{cases} \tag{5}$$

Functions $A(\ell)$ and $k(\ell)$ can be obtained for any imposed displacement, exploiting the proportionality between the stress (resp. energy) and the prescribed displacement (resp. square prescribed displacement). Once computed, the crack initiation length and the loading level are obtained using Eq. (5) for any $(\mathcal{G}_c, \sigma_c)$ couples.

2.2. Quasi-static approach for Non-linear Elastic material model

Using a NLE material model, under quasi-static loading, the stress and energy requirements can be written using the same inequalities (1) and (3) as for LE case. However, the main difference is that the stress $\sigma(\ell, U)$ and the IERR $\mathcal{G}_{inc}(\ell, U)$ become two nonlinear functions of *U* and U^2. It is thus necessary to compute the stress and energy conditions for several loading levels. The loading level at crack initiation corresponds to the minimum loading level U_c satisfying both requirements, which can be determined by solving the following minimization problem:

$$U_c = \min \left\{ U, \exists \ell, \left(\frac{\mathcal{G}_{inc}(\ell, U)}{\mathcal{G}_c} \geq 1 \right) \wedge \left(\frac{\sigma(\ell, U)}{\sigma_c} \geq 1 \right) \right\} \tag{6}$$

The initiation crack length ℓ_c is thus obtained by:

$$\min \left(\frac{\mathcal{G}_{inc}\left(\ell_c, U_c\right)}{\mathcal{G}_c}, \frac{\sigma\left(\ell_c, U_c\right)}{\sigma_c} \right) = 1 \tag{7}$$

Considering NLE material model, the CC implementation is computationally more expensive than in LE case since it requires more calculations due to the loss of proportionality of the stress (resp. the IERR) to the loading (resp. the square loading).

2.3. Dynamic approach for Linear Elastic material model

Applying the dynamic approach of the CC under quasi-static loading conditions, the stress requirement is the same as in the quasi-static approach due to the fact that the stress fields depend only on the loading magnitude. In the present work, only quasi-static loading conditions are considered [19]. In case dynamic loadings are considered, it is possible to introduce a characteristic time in the stress criterion, as proposed in [27]. The key difference between quasi-static and dynamic approach of the CC relies on the description of the crack length variation as a function of time instead of the assumption of an instantaneous process in the quasi-static approach. In the dynamic approach, the crack length jumps from 0 to the initiation crack length ℓ_c in a given time following a certain velocity profile $v_{crack}(t) = d\ell(t)/dt$.

The IERR can be written so as to consider the kinetic energy variation due to crack initiation.

$$\mathcal{G}_{inc}^{dyn}(\ell(t), U) = \frac{\Delta W_{ext}(\ell(t), U) - \Delta W_p(\ell(t), U) - \Delta W_k(\ell(t), U)}{\ell(t)} \tag{8}$$

Due to the consideration of the kinetic energy, the energy criterion now is written as an equality rather than an inequality (Eq. (3)) in the quasi-static approach. This formulation remains consistent with the quasi-static (QS) formulation when the kinetic energy variation tends towards zero. The kinetic energy is proportional to the square prescribed loading for LE case. It can be written as a function of the velocity ($\dot{u}$) field:

$$W_k = \frac{1}{2}\int_V \rho(\vec{\dot{u}} \cdot \vec{\dot{u}})dV \tag{9}$$

Therefore, the dynamic IERR for LE case is also proportional to the square prescribed loading. Furthermore, it also requires several calculations with different crack lengths at a given loading to satisfy Eq. (5), then the initiation crack length and the loading level can be determined similarly to the quasi-static approach. The implementation of the dynamic approach requires the assumption of the crack velocity profile and the material density. More details about the FE implementation of the CC dynamic approach for LE case are given in [28].

2.4. Dynamic approach for Non-linear Elastic material model

Based on the dynamic approach for LE material model, considering the nonlinearity, the stress and energy requirements can be written by using Eqs. (1) and (8). Compared to the quasi-static approach, the dynamic approach for NLE case considers the crack velocity profile $v_{crack}(t)$ instead of an instantaneous crack initiation. Meanwhile, the stress $\sigma(\ell(t), U)$ and the IERR $\mathcal{G}_{inc}^{dyn}(\ell(t), U)$ are two nonlinear functions of *U* or U^2, which is the main difference with the dynamic approach for LE case.

The dynamic approach for NLE case implementation requires an incremental procedure to compute both stress and energy requirements, similarly to the implementation of the quasi-static approach in NLE case (Section 2.2). For a given imposed displacement *U*, the stress along the crack path before crack initiation and the dynamic incremental energy release rate is calculated as described in Section 2.3. Compared to the quasi-static approach considering nonlinear elastic material model, the CC solution in the dynamic approach considering nonlinear elastic material model is obtained using a dynamic solver in order to calculate the kinetic energy variation in the energy balance. The critical loading U_c and the initiation crack length ℓ_c are determined solving Eqs. (6) and (7). For every critical loading U_c, an averaged tension applied at the side of plate is calculated as the fracture stress σ_o.

3. Numerical implementation

This section focus on the numerical implementation of the CC dynamic approach considering NLE material model. In this section, we carry out 2D implicit dynamic simulation considering nonlinear elasticity, disregarding plastic dissipation.

3.1. Hyperelastic material model

The PMMA tensile stress-strain curve, obtained in [19], is fitted by the hyperelastic Marlow model to represent PMMA nonlinear elasticity. Since no unloading processes are considered, the hyperelastic Marlow model is used to describe the material nonlinearity. The Ramberg-Osgood [19] material model could also be used to represent this material nonlinearity. The chosen material model proposed by Marlow [29], enables

reproducing a nonlinear elastic material behavior [25, 30]. The true stress and true strain values are used as a tabular input. Assuming that this material model only depends on the strain energy density, a constitutive relation is derived from uniaxial tensile test. Therefore, it only requires the uniaxial tension test data as input. The fitted curve is shown in Fig. 2 using the experimental data measured in [19]. The hyperelastic Marlow model is accurate enough to describe the nonlinearity of PMMA.

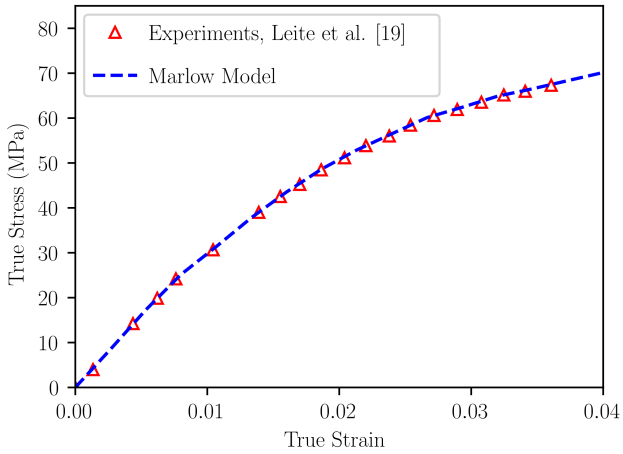

Figure 2: True stress-strain curve obtained experimentally under uniaxial tension and fitted using Marlow model.

3.2. Finite element model

The CC dynamic approach for NLE case under quasi-static loading is illustrated by studying holed PMMA plate specimens failure under tension. Due to the geometry and loading symmetry, only one quarter of the plate is modeled as shown in Fig. 3. A displacement *U* along x direction is imposed to all nodes of the right edge. Symmetry conditions are imposed on the bottom and left edge. The symmetry condition is then released for each node of the crack path to calculate the IERR. To capture accurately the variation of the energy, a fully controllable square mesh is generated. The mesh is refined near the crack path with uniform mesh size ℓ_m along the crack. The influence of ℓ_m on the energy variation is discussed in the following. The quarter circular edge of the hole is meshed by a fixed mesh size, having at least 30 elements on this side. At the other edges, an increasing mesh size configuration is used to keep a good mesh quality. The sketch of the mesh configuration is shown in Fig. 3. Linear plane stress elements with 4 nodes are used.

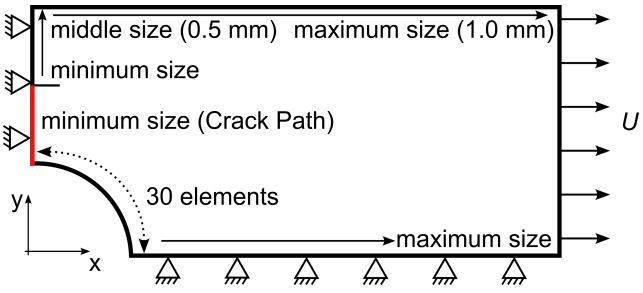

Figure 3: Schematic view of mesh size distribution.

3.3. Influence of time increments and mesh sizes for dynamic LE case

The IERR is computed by releasing Dirichlet boundary conditions of the nodes along the crack path. We first study the influence of the number of time increments during one node release step for one given constant crack velocity $v_{crack} = 500$ m/s. The IERRs are calculated using either 10, 15, 20 or 25 time increments, resulting in difference smaller than around 1%. Similar convergence results are obtained for other crack velocities. In the following, 10 increments are set for dynamic LE case.

The influence of mesh size ℓ_m on the IERR calculation is also investigated. The different mesh sizes lead to IERR differences smaller than 2%. Accordingly, we set ℓ_m = 0.02 mm along the crack path for LE case.

3.4. Influence of damping ratio, time increments and mesh size for NLE case

Numerical damping is used to reduce the high frequency oscillations due to the Dirichlet condition release [31]. However, it must be ensured that the use of damping does not influence the value of the IERR. Fig. 4 shows the IERR variation as a function of the crack length and several damping coefficients β for $v_{crack} = 500$ m/s crack velocity. The IERR for damping ratio $\beta \leqslant 10^{-5}/v_{crack}$ is close to that without considering damping. We thus set $\beta v_{crack} = 10^{-5}$ mm in the following calculation. Due to the nonlinearity, the potential energy is smaller than that obtained for LE case from quasi-static approach [19]. Furthermore, in the CC dynamic approach, it is shown that the larger the crack velocity, the smaller the potential energy difference and the larger the kinetic energy difference [28]. Therefore, the IERR is smaller when the crack velocity is larger, which leads to an increase in the initiation crack length. We study the influence of time increments and mesh sizes on the IERR for NLE case for a given constant crack velocity $v_{crack} = 100$ m/s. The IERRs are calculated using 10, 15, or 20 time increments, resulting in difference smaller than 5%. Therefore, 10 increments per node unbuttoning for NLE case are used in the following.

The influence of the mesh size ℓ_m on the IERR is also investigated. The maximum difference of IERRs for $\ell_m = 0.01$ mm and 0.02 mm obtained using Eq. (8) from the FE solution for $v_{crack} = 100$ m/s is smaller than 2 %. Similar convergence results are obtained for other crack velocities. We thus set ℓ_m = 0.02 mm along the crack path for NLE case. Fig. 5 shows the IERR variation as a function of crack length for several crack velocities as well as the dynamic to quasi-static IERR ratios $\mathcal{G}_{inc}^{dyn}/\mathcal{G}_{inc}^{qs}$ as a function of crack velocity for NLE case. For small crack velocities, for example $v_{crack} = 100$ and 300 m/s, the IERR increases with increasing crack length. For larger crack velocity, the IERR increases to a peak value at first and after a decrease, it increases again. For a semi-infinite crack in the infinite plate made of a linear elastic material, the dynamic to quasi-static IERR ratio shows a quasi-linear variation as a function of the crack velocity [32]. However, for NLE case, we find that this variation is significantly nonlinear, as shown in Fig. 5(b). The larger the crack velocity, the smaller the variation of the IERR as a function of the crack velocity.

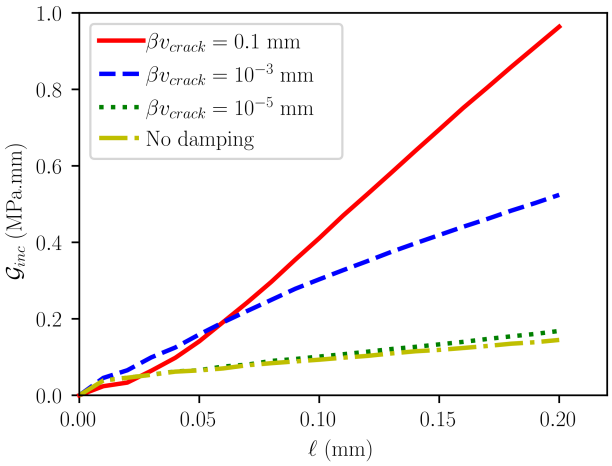

Figure 4: Energy release rate as a function of crack length for $v_{crack} = 500$ m/s and several damping coefficients β.

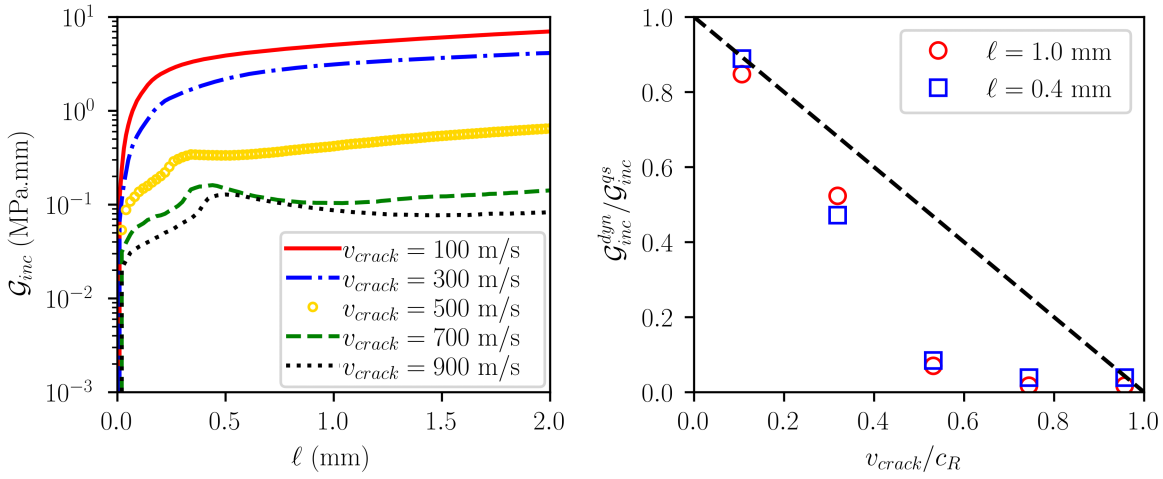

(a) (b)

Figure 5: (a) Energy release rate as a function of crack length for several crack velocities for NLE case and (b) Dynamic to quasi-static incremental energy release rate ratio as a function of normalized crack velocity for two different crack lengths.

4. Circular hole specimen under tensile loading

We now study crack initiation in a circular holed specimen under tensile loading. An example of the CC dynamic approach implementations for LE case and NLE case are presented for ϕ = 2 mm hole diameter, the results being qualitatively similar for other hole radii. Then, the results for all diameters are compared with the experimental results observed in [19]. Finally, the influence of the velocity profile on the predicted fracture stress is studied.

4.1. Crack initiation from circular hole with 2 mm diameter

4.1.1. CC dynamic approach for LE case

The CC dynamic approach under quasi-static loading requires the calculation of the stress and the energy criteria. Fig. 6(a) shows the CC solution for several crack velocities. The initiation crack length increases with

increasing crack velocities, and the initiation displacement U_c (or equivalently fracture stress) increases with increasing crack velocities, as shown in Table 2, which are in good agreement with results obtained in [28]. The initiation stress measured experimentally [19] ranges from 50 MPa to 56 MPa for ϕ = 2 mm, which is well reproduced numerically for a crack velocity range v_{crack} varying from 730 m/s to 770 m/s. This crack velocity is in the order of magnitude of experimentally measured crack velocities in PMMA [19, 33].

Crack velocity (m/s)	300	400	500	600	700	730	770	800
Initiation displacement (mm)	1.55	1.65	1.9	2.0	2.4	2.55	2.75	2.98
Fracture stress (MPa)	30.98	32.97	37.97	39.97	47.96	50.96	54.96	59.55

Table 2: Initiation displacement U_c and failure stress σ_0 obtained for several crack velocities

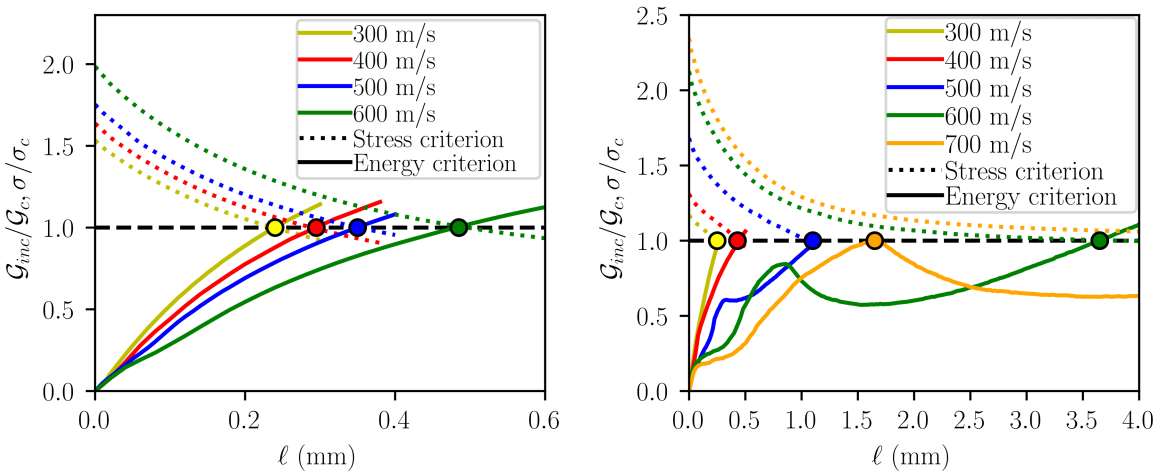

(a) (b)

Figure 6: Stress and energy criteria as a function of the crack length for several crack velocities (a) for LE case and (b) for NLE case.

4.1.2. CC dynamic approach for NLE case

Considering PMMA nonlinear elasticity, the IERR variation shows an overall increasing trend as a function of the crack length for small crack velocities. For large enough crack velocity, the IERR increases to a peak value and after decreasing, continues to increase again. Thus, the initiation crack length increases with an increasing crack velocity as shown in Fig. 6(b) for v_{crack} ranging from 300 m/s to 700 m/s. When $v_{crack} = 700$ m/s, the initiation crack length decreases strongly. In this case, crack initiation is controlled only by the energy criterion and the stress criterion $\sigma > \sigma_c$ is fulfilled along the crack path ($\ell \leqslant \ell_c$) (Fig. 6(b)).

Due to the smaller IERR for NLE case compared to LE case, the fracture stress σ_0 is larger for a same crack velocity as for LE case. Therefore, a small prescribed crack velocity is required to obtain the same fracture stress. It varies from 500 m/s to 550 m/s to obtain the fracture stress range measured experimentally for ϕ = 2 mm hole diameter [19]. The crack velocity range is similar to the ones obtained using LE material model, but the velocity magnitude is smaller.

4.2. Comparison with experimental results for all diameters

Fig. 7(a) shows the initiation stress variation as a function of the specimen hole diameter obtained numerically for LE material model or experimentally [19]. As explained previously, the CC quasi-static approach for LE case underestimates the initiation stress compared to experimental results. The predicted initiation stress increases with increasing crack velocities. However, assuming a constant initiation crack velocity, whatever the hole diameter does not allow retrieving quantitatively the failure stress variation measured experimentally for all hole diameters. For different diameters, a corresponding range of the crack velocity can be computed to well reproduce the experimental results, which is shown in Fig. 7(b). It can be observed that the larger the diameter, the larger the identified crack velocity.

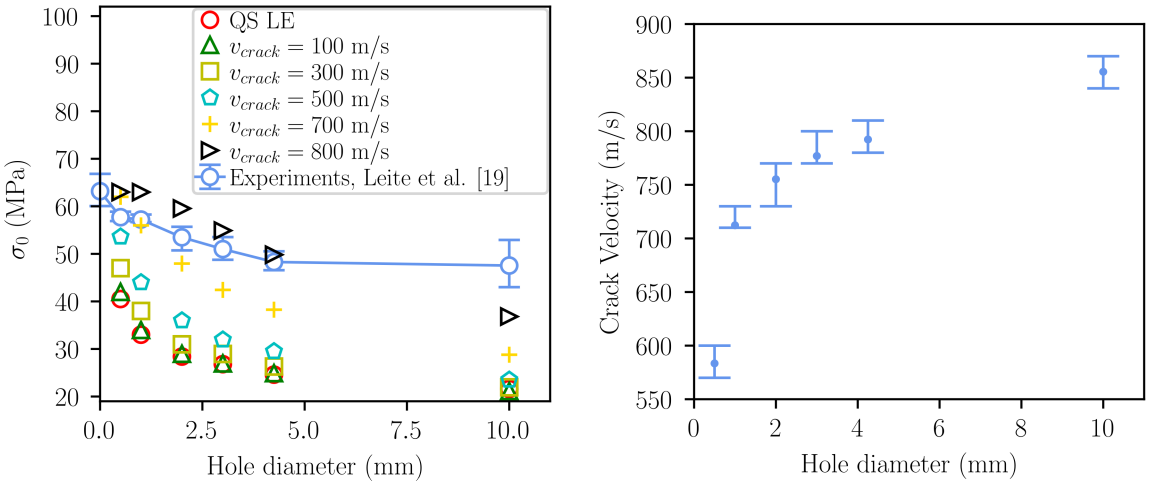

(a) (b)

Figure 7: (a) Comparison of failure stress obtained numerically considering LE material model for different crack velocities and experimentally [19] and (b) Range of crack velocities to reproduce the experimental results using CC dynamic approach for LE case, for several hole diameters.

Fig. 8(a) shows a comparison of the predicted fracture stresses obtained experimentally in [19] and considering NLE material model. Similar qualitative trends as for LE case are obtained. The failure stresses obtained under QS assumption underestimate the ones measured experimentally and no quantitative agreement is obtained assuming a constant crack velocity for all diameters. The range of crack velocities to reproduce the experimental results using CC dynamic approach for NLE case for several hole diameters is shown in Fig. 8(b). Similarly to LE material model, the range of crack velocities also increases with increasing hole diameters. However, the velocity magnitude is smaller than for LE material model, still in the order of magnitude of crack velocities measured experimentally. In particular, for ϕ = 10 mm, the fracture stress measured experimentally by Leite et al. [19] ranges from 43 MPa to 53 MPa and the mean value is 47 MPa. The crack velocity obtained by CC dynamic approach for NLE case corresponding to the minimum experimental value (43 MPa) is 800 m/s, whereas the crack velocity corresponding to the mean value (47 MPa) would be 1500 m/s. Indeed, crack initiation is only driven by the energy requirement for $v_{crack} > 700$ m/s, and the IERR for ϕ = 10 mm is smaller than that for other diameters, which leads to a variation range of corresponding crack velocities larger than

those measured experimentally. Note that using a 600m/s crack velocity, the predicted failure stress for this hole size would be 38 MPa, which slightly underestimates the values obtained experimentally.

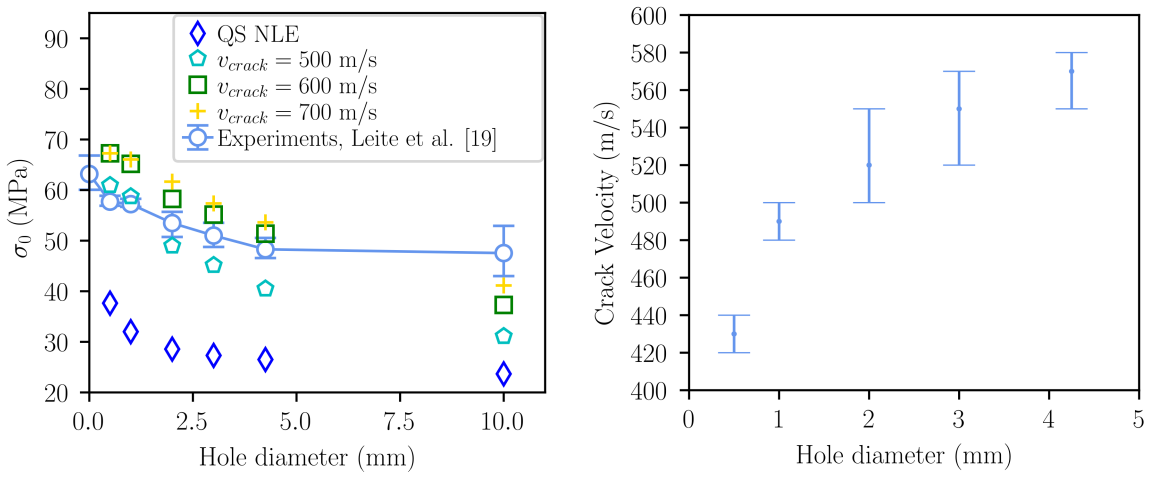

(a) (b)

Figure 8: (a) Comparison of σ_c obtained experimentally [19] and (b) the range of crack velocity to reproduce the experimental results with the CCFFM predictions using CC dynamic approach for NLE case, for several hole diameters.

4.3. *Influence of velocity profile*

The previous results were obtained assuming a constant crack velocity, whereas the actual crack velocity may vary during crack initiation [19, 33, 34]. We choose the following description of the velocity profile as a function of time to describe a possible increasing crack velocity during initiation:

$$v_{crack}(t) = \alpha v_0 \left(\frac{t}{t_c^1}\right)^{\alpha-1} \quad (1 \leq \alpha \leq 2) \tag{10}$$

where $t_c^1 = \ell_c^1/v_0$, and ℓ_c^1 is obtained for a constant crack velocity v_0, which guarantees that the mean velocity $\overline{v} = \frac{1}{t_c^1}\int_0^{t_c^1} v_{crack}(t)dt$ during the crack initiation ([0, t_c^1]) is v_0 for different velocity profiles. Thus, ℓ_c^1, v_0 and t_c^1 will vary for different hole diameters ϕ and different imposed displacements U. In particular, for $\alpha = 1.0$, we retrieve a constant crack velocity profile; for $\alpha = 1.5$, the crack velocity is $v_{crack}(t) = 1.5v_0\left(t/t_c^1\right)^{0.5}$, called the square root (SQRT) velocity profile; for $\alpha = 2.0$, the crack velocity is $v_{crack}(t) = 2v_0\left(t/t_c^1\right)$, called the linear velocity profile. Fig. 9 shows the variation of the crack length ℓ and the crack velocity v_{crack} as a function of time for several α values.

Experimental observations reveal that crack branching emerging from the main crack may occur if the crack velocity reaches a critical crack velocity $v_{crack} \approx 0.6c_R$, where c_R is the Rayleigh velocity. Disregarding a possible crack branching, it can thus be assumed that the crack velocity during initiation remains smaller than $0.6c_R$ (the red dashed lines in Fig. 9 exhibit slopes equal to $0.6c_R$). The maximum velocity obtained for the proposed velocity profile (Eq. (10)) is αv_0. Therefore, the constant crack velocity verifies $v_0 \leq 0.6c_R/\alpha$.

For LE case, Fig. 10(a) shows the stress and energy criteria as a function of the crack length corresponding to α = 1.0, 1.5 and 2.0 for v_0 = 300 m/s and ϕ = 2.0 mm. The initiation crack lengths are indicated by red

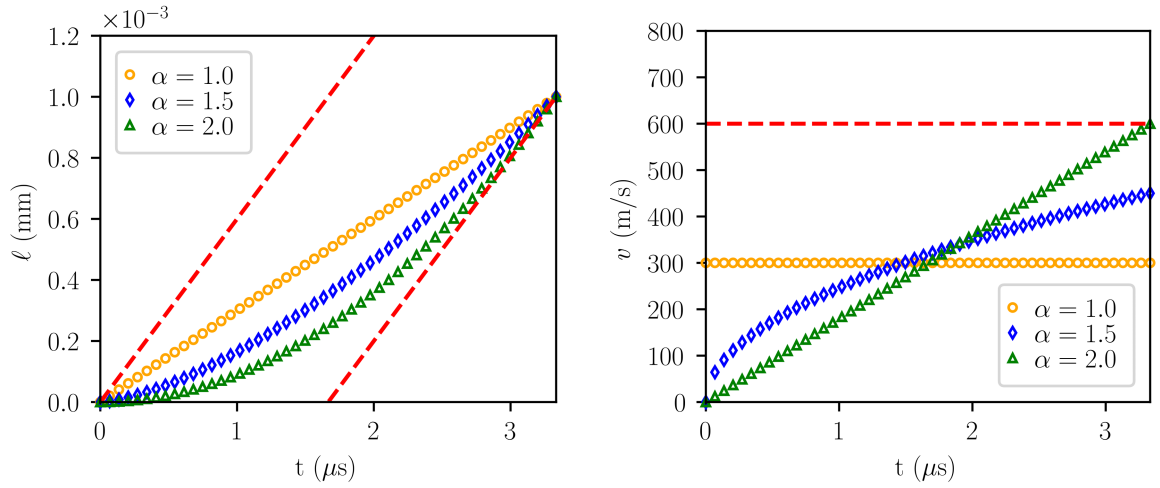

(a) (b)

Figure 9: (a) Variation of the crack length and (b) the crack velocity with time for different α (The dashed red lines represent the limit imposed by the Rayleigh velocity.).

dashed lines. Fig. 10(b) shows the variation of the crack length ℓ with time for v_0 = 300 m/s and for different α values. Circles in Fig. 10(b) indicate the initiation crack length ℓ_c determined by CC dynamic approach and the corresponding time t_c obtained for different velocity profiles. The initiation crack lengths ℓ_c for different α slightly vary depending on the velocity profile but remain in the same order of magnitude as the initiation crack length (ℓ_c^1) obtained for a constant crack velocity. Therefore, the actual mean crack velocity during crack initiation ([0, t_c]) also remains in the same order of magnitude as for the constant velocity profile. For instance, it varies between 300 m/s and 343 m/s for alpha between 1.0 and 2.0 (Fig. 10(b)). Since the maximum velocity is bounded by $0.6c_R$, the velocity profile can be varied in a certain range of α which is larger for smaller crack velocities. For a given mean crack velocity, the fracture stress increases with increasing α, thus highlighting a non negligible influence of the velocity profile (Fig. 10(c)). Similar influence of the crack velocity profile on the fracture stress is obtained for NLE material model.

5. Conclusion

We extend the CC dynamic approach taking into account nonlinear elasticity. Compared to the previous CC approaches, the main difference lies in considering the kinetic energy variation due to crack initiation following a certain velocity profile in a nonlinear elastic material under quasi-static loading. Accordingly, the potential and kinetic energies are no longer proportional to the prescribed loading or the square prescribed loading. For a large constant crack velocity, the variation of IERR as a function of the crack length exhibits a peak value and the IERR decreases nonlinearly with an increasing crack velocity.

Using either LE or NLE material model, the CC dynamic approach improves the underestimation of the fracture stress variation as a function of the hole diameter obtained using the quasi-static approach. A quantitative agreement with experiments is not obtained assuming the same constant crack velocity for all the hole

diameters. Assuming constant crack velocity during crack initiation, the larger the crack velocity, the larger the predicted fracture stress. A good quantitative agreement of the predicted and measured fracture stress is obtained by inputting increasing crack velocity with increasing hole diameter. Similar qualitative trends are obtained using NLE material model, the identified crack velocities being smaller than for LE material model.

The crack velocity profile has a non-negligible influence on the predicted fracture stress. Future works will cover the crack velocity profile determination during crack initiation.

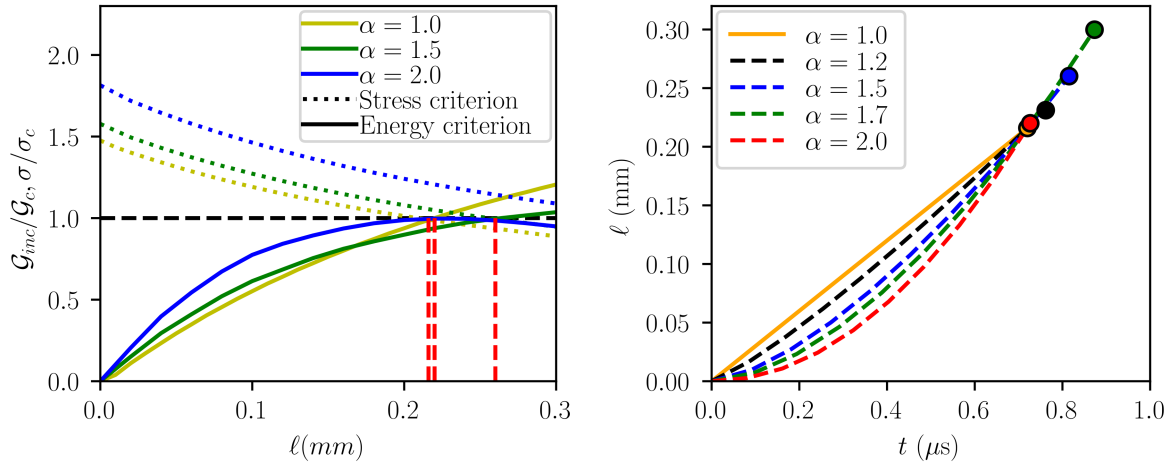

(a) (b)

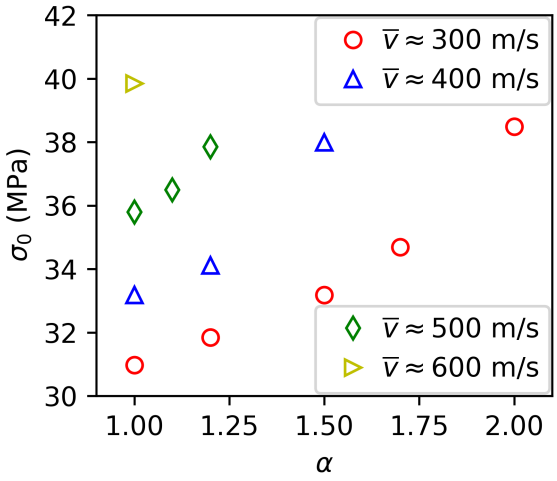

(c)

Figure 10: (a) Stress and energy criteria as a function of the crack length corresponding to α = 1.0, 1.5 and 2.0 and (b) Crack length for constant crack velocity v_0 = 300 m/s, ϕ = 2.0 mm and different α (circles indicate the initiation crack length ℓ_c and the corresponding time t_c) and (c) fracture stresses for different crack velocities and different α for LE case.

Declaration of Competing Interest

The authors declare no conflicts of interest.

Acknowledgements

This work was supported by the China Scholarship Council (CSC) (Xi CHEN).

References

[1] Z. Hashin, Finite thermoelastic fracture criterion with application to laminate cracking analysis, Journal of the Mechanics and Physics of Solids 44 (7) (1996) 1129–1145. doi:https://doi.org/10.1016/0022-5096(95)00080-1.

[2] J. Nairn, Exact and variational theorems for fracture mechanics of composites with residual stresses, traction-loaded cracks, and imperfect interfaces, International Journal of Fracture 105 (2000) 243–271. doi:10.1023/A:1007666426275.

[3] A. A. Griffith, G. I. Taylor, Vi. the phenomena of rupture and flow in solids, Philosophical Transactions of the Royal Society of London. Series A, Containing Papers of a Mathematical or Physical Character 221 (582-593) (1921) 163–198. doi:10.1098/rsta.1921.0006.

[4] D. Leguillon, Strength or toughness? a criterion for crack onset at a notch, European Journal of Mechanics - A/Solids 21 (1) (2002) 61–72. doi:https://doi.org/10.1016/S0997-7538(01)01184-6.

[5] P. Cornetti, N. Pugno, A. Carpinteri, D. Taylor, Finite fracture mechanics: A coupled stress and energy failure criterion, Engineering Fracture Mechanics 73 (14) (2006) 2021–2033. doi:https://doi.org/10.1016/j.engfracmech.2006.03.010.

[6] A. Doitrand, A. Sapora, Nonlinear implementation of finite fracture mechanics: A case study on notched brazilian disk samples, International Journal of Non-Linear Mechanics 119 (2020) 103245. doi:https://doi.org/10.1016/j.ijnonlinmec.2019.103245.

[7] P. Cornetti, A. Sapora, A. Carpinteri, Short cracks and v-notches: Finite fracture mechanics vs. cohesive crack model, Engineering Fracture Mechanics 168 (2016) 2–12. doi:https://doi.org/10.1016/j.engfracmech.2015.12.016.

[8] D. Leguillon, Z. Yosibash, Failure initiation at v-notch tips in quasi-brittle materials, International Journal of Solids and Structures 122-123 (2017) 1–13. doi:https://doi.org/10.1016/j.ijsolstr.2017.05.036.

[9] V. Mantič, I. García, Crack onset and growth at the fibre–matrix interface under a remote biaxial transverse load. application of a coupled stress and energy criterion, International Journal of Solids and Structures 49 (17) (2012) 2273–2290. doi:https://doi.org/10.1016/j.ijsolstr.2012.04.023.

[10] N. Stein, P. Weißgraeber, W. Becker, A model for brittle failure in adhesive lap joints of arbitrary joint configuration, Composite Structures 133 (2015) 707–718. doi:https://doi.org/10.1016/j.compstruct.2015.07.100.

[11] P. Weißgraeber, D. Leguillon, W. Becker, A review of finite fracture mechanics: crack initiation at singular and non-singular stress raisers, Archive of Applied Mechanics 86 (1) (2016) 375–401. doi:https://doi.org/10.1007/s00419-015-1091-7.

[12] A. Sapora, P. Cornetti, Crack onset and propagation stability from a circular hole under biaxial loading, International Journal of Fracture 214 (1) (2018) 97–104. doi:https://doi.org/10.1007/s10704-018-0315-6.

[13] P. Rosendahl, P. Weißgraeber, N. Stein, W. Becker, Asymmetric crack onset at open-holes under tensile and in-plane bending loading, International Journal of Solids and Structures 113-114 (2017) 10–23. doi:https://doi.org/10.1016/j.ijsolstr.2016.09.011.

[14] A. Chao Correas, M. Corrado, A. Sapora, P. Cornetti, Size-effect on the apparent tensile strength of brittle materials with spherical cavities, Theoretical and Applied Fracture Mechanics 116 (2021) 103120. doi:https://doi.org/10.1016/j.tafmec.2021.103120.

[15] T. Laschuetza, T. Seelig, Remarks on dynamic cohesive fracture under static pre-stress — with a comparison to finite fracture mechanics, Engineering Fracture Mechanics 242 (2021) 107466. doi:https://doi.org/10.1016/j.engfracmech.2020.107466.

[16] A. Doitrand, D. Leguillon, Asymptotic analysis of pore crack initiation near a free edge, Theoretical and Applied Fracture Mechanics 116 (2021) 103125. doi:https://doi.org/10.1016/j.tafmec.2021.103125.

[17] J. Li, X. Zhang, A criterion study for non-singular stress concentrations in brittle or quasi-brittle materials, Engineering Fracture Mechanics 73 (4) (2006) 505–523. doi:https://doi.org/10.1016/j.engfracmech.2005.09.001.

[18] A. Sapora, A. Torabi, S. Etesam, P. Cornetti, Finite fracture mechanics crack initiation from a circular hole, Fatigue & Fracture of Engineering Materials & Structures 41 (7) (2018) 1627–1636. doi:https://doi.org/10.1111/ffe.12801.

[19] A. Leite, V. Mantič, F. París, Crack onset in stretched open hole pmma plates considering linear and non-linear elastic behaviours, Theoretical and Applied Fracture Mechanics 114 (2021) 102931. doi:https://doi.org/10.1016/j.tafmec.2021.102931.

[20] A. R. Torabi, F. Berto, A. Sapora, Finite fracture mechanics assessment in moderate and large scale yielding regimes, Metals 9 (5). doi:10.3390/met9050602.

[21] A. T. l'Armée, S. Hell, P. Rosendahl, J. Felger, W. Becker, Nonlinear crack opening integral: Mode mixity for finite cracks, Engineering Fracture Mechanics 186 (2017) 283–299. doi:https://doi.org/10.1016/j.engfracmech.2017.10.006.

[22] X. Wei, H.-S. Shen, H. Wang, Effect of interfacial energy combined with geometrical nonlinearity on the finite fracture analysis of composite single-lap joints, Composite Structures 280 (2022) 114938. doi:https://doi.org/10.1016/j.compstruct.2021.114938.

[23] D. Leguillon, Z. Yosibash, Failure initiation at v-notch tips in quasi-brittle materials, International Journal of Solids and Structures 122-123 (2017) 1–13. doi:https://doi.org/10.1016/j.ijsolstr.2017.05.036.

[24] Z. Yosibash, V. Mendelovich, I. Gilad, A. Bussiba, Can the finite fracture mechanics coupled criterion be applied to v-notch tips of a quasi-brittle steel alloy?, Engineering Fracture Mechanics 269 (2022) 108513. doi:https://doi.org/10.1016/j.engfracmech.2022.108513.

[25] P. Rosendahl, Y. Staudt, A. Schneider, J. Schneider, W. Becker, Nonlinear elastic finite fracture mechanics: Modeling mixed-mode crack nucleation in structural glazing silicone sealants, Materials and Design 182 (2019) 108057. doi:https://doi.org/10.1016/j.matdes.2019.108057.

[26] J. Le Pavic, T. Bonnemains, É. Lolive, G. Stamoulis, D. Da Silva, D. Thévenet, Failure load prediction of a tubular bonded structures using a coupled criterion, Theoretical and Applied Fracture Mechanics 108 (2020) 102531. doi:https://doi.org/10.1016/j.tafmec.2020.102531.

[27] A. Chao Correas, P. Cornetti, M. Corrado, A. Sapora, Finite fracture mechanics extension to dynamic loading scenarios, International Journal of Fracturedoi:10.1007/s10704-022-00655-x.

[28] A. Doitrand, G. Molnár, D. Leguillon, E. Martin, N. Carrère, Dynamic crack initiation assessment with the coupled criterion, European Journal of Mechanics-A/Solids 93 (2022) 104483. doi:https://doi.org/10.1016/j.euromechsol.2021.104483.

[29] R. Marlow, A general first-invariant hyperelastic constitutive model, Constitutive Models for Rubber (2003) 157–160.

[30] R. Tobajas, E. Ibartz, L. Gracia, A comparative study of hyperelastic constitutive models to characterize the behavior of a polymer used in automotive engines, in: Proceedings of the 2nd International Electronic Conference on Materials, Vol. 2, MDPI Basel, Switzerland, 2016, p. A002.

[31] B. Croquelois, J. Kopp, J. Girardot, P. Tchoreloff, V. Mazel, Dynamic fracture analysis in brazilian test: application to pharmaceutical tablets, International Journal of Fracture 229 (1) (2021) 113–124. doi:https://doi.org/10.1007/s10704-021-00544-9.

[32] L. B. Freund, Dynamic fracture mechanics, Cambridge university press, 1998.

[33] I. Smirnov, N. Kazarinov, Y. Petrov, Experimental observation and numerical modelling of unstable behaviour of a fast crack velocity, Theoretical and Applied Fracture Mechanics 101 (2019) 53–58. doi:https://doi.org/10.1016/j.tafmec.2019.02.006.

[34] E. Bura, A. Seweryn, Mode i fracture in pmma specimens with notches – experimental and numerical studies, Theoretical and Applied Fracture Mechanics 97 (2018) 140–155. doi:https://doi.org/10.1016/j.tafmec.2018.08.002.